A Letters Journal Exploring the Frontiers of Physics

OFFPRINT

Anisotropic Zeeman shift in p-type GaAs quantum point contacts

Y. Komijani, M. Csontos, I. Shorubalko, U. Zülicke, T. Ihn, K. Ensslin, D. Reuter and A. D. Wieck

EPL, **102** (2013) 37002

epl

A Letters Journal Exploring the Frontiers of Physics

AN INVITATION TO SUBMIT YOUR WORK

www.epljournal.org

The Editorial Board invites you to submit your letters to EPL

EPL is a leading international journal publishing original, high-quality Letters in all areas of physics, ranging from condensed matter topics and interdisciplinary research to astrophysics, geophysics, plasma and fusion sciences, including those with application potential.

The high profile of the journal combined with the excellent scientific quality of the articles continue to ensure EPL is an essential resource for its worldwide audience. EPL offers authors global visibility and a great opportunity to share their work with others across the whole of the physics community.

Run by active scientists, for scientists

EPL is reviewed by scientists for scientists, to serve and support the international scientific community. The Editorial Board is a team of active research scientists with an expert understanding of the needs of both authors and researchers.

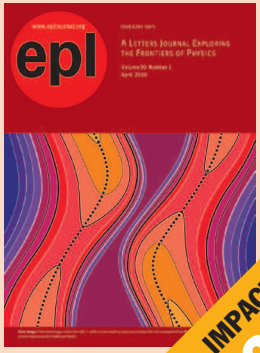

IMPACT FACTOR 2.753*

*As ranked by ISI 2010

IMPACT FACTOR
2.753*
* As listed in the ISI® 2010 Science Citation Index Journal Citation Reports

OVER
500 000
full text downloads in 2010

30 DAYS
average receipt to online publication in 2010

16 961
citations in 2010
37% increase from 2007

"We've had a very positive experience with EPL, and not only on this occasion. The fact that one can identify an appropriate editor, and the editor is an active scientist in the field, makes a huge difference."

Dr. Ivar Martinv
Los Alamos National Laboratory, USA

Six good reasons to publish with EPL

We want to work with you to help gain recognition for your high-quality work through worldwide visibility and high citations.

1. **Quality** – The 40+ Co-Editors, who are experts in their fields, oversee the entire peer-review process, from selection of the referees to making all final acceptance decisions
2. **Impact Factor** – The 2010 Impact Factor is 2.753; your work will be in the right place to be cited by your peers
3. **Speed of processing** – We aim to provide you with a quick and efficient service; the median time from acceptance to online publication is 30 days
4. **High visibility** – All articles are free to read for 30 days from online publication date
5. **International reach** – Over 2,000 institutions have access to EPL, enabling your work to be read by your peers in 100 countries
6. **Open Access** – Articles are offered open access for a one-off author payment

Details on preparing, submitting and tracking the progress of your manuscript from submission to acceptance are available on the EPL submission website **www.epletters.net**.

If you would like further information about our author service or EPL in general, please visit **www.epljournal.org** or e-mail us at **info@epljournal.org**.

EPL is published in partnership with:

European Physical Society | Società Italiana di Fisica | EDP Sciences | IOP Publishing

epl A Letters Journal Exploring the Frontiers of Physics

May 2013

EPL, **102** (2013) 37002 www.epljournal.org
doi: 10.1209/0295-5075/102/37002

Anisotropic Zeeman shift in p-type GaAs quantum point contacts

Y. Komijani[1(a)], M. Csontos[1(b)], I. Shorubalko[1,2], U. Zülicke[3], T. Ihn[1], K. Ensslin[1], D. Reuter[4(c)] and A. D. Wieck[4]

[1] *Solid State Physics Laboratory, ETH Zurich - 8093 Zurich, Switzerland*
[2] *Electronics/Metrology/Reliability Laboratory, EMPA - 8600 Duebendorf, Switzerland*
[3] *School of Chemical and Physical Sciences and MacDiarmid Institute for Advanced Materials and Nanotechnology, Victoria University of Wellington - Wellington 6140, New Zealand*
[4] *Angewandte Festkörperphysik, Ruhr-Universität Bochum - 44780 Bochum, Germany, EU*

received 8 February 2013; accepted 15 April 2013
published online 13 May 2013

PACS 73.23.Ad – Ballistic transport
PACS 73.63.Nm – Electronic transport in nanoscale materials and structures: Quantum wires
PACS 71.70.Ej – Spin-orbit coupling, Zeeman and Stark splitting, Jahn-Teller effect

Abstract – Low-temperature electrical conductance spectroscopy measurements of quantum point contacts implemented in p-type GaAs/AlGaAs heterostructures are used to study the Zeeman splitting of 1D subbands for both in-plane and out-of-plane magnetic field orientations. The resulting in-plane g-factors agree qualitatively with those of previous experiments on quantum wires while the quantitative differences can be understood in terms of the enhanced quasi-1D confinement anisotropy. The influence of confinement potential on the anisotropy is discussed and an estimate for the out-of-plane g-factor is obtained which, in contrast to previous experiments, is close to the theoretical prediction.

Introduction. – A magnetic field changes the energy of an electron by coupling to its magnetic moment, according to

$$\Delta E_{\uparrow\downarrow} = g^* \mu_B B, \tag{1}$$

an effect known as the Zeeman splitting. Here $\mu_B = \hbar e/2m_0 \approx 58\ \mu$eV/T is the Bohr magneton and m_0 is the free-electron mass. For a free electron in vacuum $g = 2$, while in a solid-state environment the spin-orbit interaction (SOI) strongly modifies the Zeeman shift [1]. As a result, for conduction band electrons in bulk GaAs, the g-factor is equal to $g^*_{\text{n-GaAs}} = -0.44$ [2].

A much richer spin physics is expected in spin-(3/2) (valence band) hole systems [3]. In bulk GaAs, the top of the valence band is composed of heavy holes (HHs), and light holes (LHs), which are degenerate at $\vec{k} = 0$. In two-dimensional hole gases (2DHGs) the quantum confinement causes an energy splitting between LHs and HHs, thereby making the growth direction the preferred direction of spin quantization for the HHs, the majority carriers at moderate densities [3]. As a result, Zeeman splitting is significant for fields perpendicular to the plane while it is expected to be zero for in-plane magnetic fields ($B_\parallel$) in quantum wells (QWs) grown on high-symmetry (001) and (111) surfaces as the Zeeman splitting has to compete with the HH-LH splitting [4,5]. Another interesting property of the valence band is that states having a finite in-plane $\vec{k}_\parallel$ are no longer pure HHs but contain admixtures from the LHs (which have a non-zero in-plane g-factor) and therefore, the in-plane g-factor is finite for finite densities even if it is zero at the subband edge. Moreover, any further confinement changes this HH-LH mixing, modifying the anisotropy of the in-plane Zeeman splitting.

While the g-factor measurements in 2D rely on the involved techniques of subband depopulation or the method of coincidence measurement based on Shubnikov-de Haas oscillations acquired at different angles [6], in ballistic systems with lower dimensions the subband structure provides direct information about the Zeeman spin-splitting. Therefore, 1D confined nano-structures are the natural choice for studying these effects. Recent technological

(a) Present address: Department of Physics and Astronomy, University of British Columbia - Vancouver, B.C., Canada V6T 1Z1; E-mail: komijani@phas.ubc.ca
(b) Present address: Department of Physics, Budapest University of Technology and Economics - 1111 Budapest, Hungary, EU.
(c) Present address: University Paderborn, Department Physik - Warburger Straße 100, 33098 Paderborn, Germany, EU.

developments have enabled the fabrication of stable hole-based nano-structures in p-type GaAs leading to the observations of a plethora of new features, exemplified by the anisotropic Zeeman shift in 1D systems, discussed here.

The first evidence for unusual spin physics in p-type nano-structures was observed on quantum wires made in a 2DHG grown on (311) surface of GaAs. In their 1D system Danneau *et al.* [7] observed that the spin degeneracy is lifted when the in-plane magnetic field $B_{\|}$ is applied parallel to the quantum wire. When $B_{\|}$ was oriented perpendicular to the wire; however, no spin splitting was observed. The authors associated this result with the importance of quantum confinement in spin-(3/2) systems.

Motivated by this work, similar experiments were performed on quantum point contacts (QPCs) [8] and quantum wires [9] fabricated on 2DHGs grown along the (311) surface of GaAs with contradictory conclusions attributing the anisotropy to both crystallographic anisotropy and confinement and suggested that the role of confinement anisotropy might be different in quantum wires and QPCs. Moreover, it motivated to repeat these experiments on nano-structures made from high-symmetry QWs where the crystallographic anisotropy does not play a role. Recently Chen *et al.* [10] did similar experiments on quantum wires fabricated on a (001)-oriented heterostructure and reported similar confinement anisotropy of the hole g-factor[1].

We have measured the Zeeman splitting in eight QPCs defined by both AFM [11] and e-beam lithography techniques in the so-called In-Plane-Gate technology [12]. They were oriented along either [110] or [1$\bar{1}$0] directions on the (001)-plane of a p-type GaAs/AlGaAs heterostructure. No dependence of the g-factor on the orientation of the QPC axis along these two crystallographic directions was observed as expected from symmetry considerations. The g-factors extracted from our experiment agree qualitatively with those reported in refs. [7,9] and [10]. We observe clear spin-splitting, if the in-plane magnetic field $B_{\|}$ is applied parallel to the QPC axis, while no spin-splitting is observed when $B_{\|}$ is perpendicular to the QPC axis. Since the measured QPCs have lithographical lengths comparable to their widths, it is remarkable to observe such a significant spin effect due to their lateral confinement. Furthermore, the emergence of the effect in QPCs, which are less ideal 1D systems than quantum wires, points to the universality of the effect and places less stringent constraints on the mobility.

Experimental details. – In this article we present data from three nominally identical QPCs fabricated with e-beam lithography and shallow wet chemical etching in three different directions of the same chip (inset of fig. 1(a)). These QPCs called *QPC1*, *QPC2* and *QPC3* have the lithographical width of 230 nm and are oriented under an angle of 45°, 0° and 90° with respect to the external in-plane magnetic field. The host heterostructure is grown on the (001)-plane of GaAs and is doped with carbon [13] serving as the acceptor for the 2DHG situated 45 nm below the surface. Prior to sample fabrication the quality of the 2DHG was characterized by standard magnetotransport measurements at 4.2 K. A hole density of $n = 4\times10^{11}$ cm^{-2}, and a mobility of $\mu = 200000$ cm^2/Vs were obtained. Further details about the fabrication process can be found in [14].

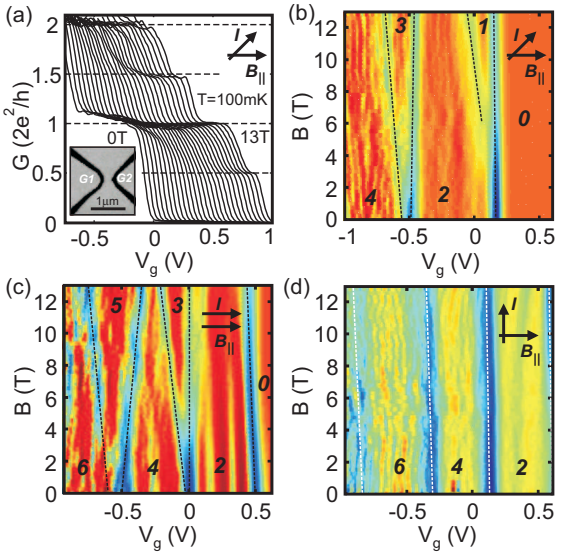

Fig. 1: (Color online) (a) Linear conductance of *QPC1* as a function of the gate voltage in in-plane magnetic fields from 0 to 13 T. The orientation of the $B_{\|}$ with respect to the current is indicated in the upper-right corner. (b)–(d): transconductance (numerical derivative of the linear conductance with respect to the gate voltage) in arbitrary units as a function of the gate voltage and in-plane magnetic field at $T = 100$ mK for *QPC1* (45° with respect to the magnetic field), *QPC2* (parallel to the magnetic field) and *QPC3* (perpendicular to the magnetic field). The (blue) high-transconductance regimes marked by the dashed lines indicate the subbands. The corresponding linear-conductances values are indicated in units of e^2/h.

Results and discussion. – Figure 1(a) shows the linear conductance G of *QPC1* at $T = 100$ mK as the in-plane magnetic field is varied from 0 to 13 T. A constant resistance, attributed to the resistance of the leads, is subtracted from the raw four-terminal measured resistances to raise the first plateau to $2e^2/h$. The zero-field conductance steps of height $2e^2/h$ evolve to spin-resolved steps of height e^2/h at $B = 13$ T due to the Zeeman splitting. It is convenient to follow this evolution on the color map of the

[1]We had already observed this effect in a number of QPCs when the paper in [10] first appeared.

Table 1: Spin-splitting of the subbands evaluated from the gate voltage dependence of the data presented in fig. 1. $V_g(n)$ denotes the gate voltage at which the n-th subband crosses the Fermi energy. The numbers in parentheses are the errors. An upper bound for the splitting is indicated for the cases where a clear spin-splitting is not observed.

	QPC1	*QPC2*	*QPC3*
$\mathrm{d}V_g(1)/\mathrm{d}B$ (mV/T)	13(±1)	<1	
$\mathrm{d}V_g(2)/\mathrm{d}B$ (mV/T)	13(±1)	17(±2)	<1
$\mathrm{d}V_g(3)/\mathrm{d}B$ (mV/T)		24(±2)	<2
$\mathrm{d}V_g(4)/\mathrm{d}B$ (mV/T)			<2

transconductance ($\mathrm{d}G/\mathrm{d}V_g$), shown in fig. 1(b), obtained as the numerical derivative of the measured linear conductance with respect to the gate voltage. Figures 1(c), (d) provide similar data for the other two QPCs. The signature of spin-splitting can be seen in these figures where the high-transconductance regimes shown in blue indicate the onset of the conductance through the next higher subband while the yellow, orange and red areas indicate the plateaus or shoulders. A clear Zeeman splitting is observed for *QPC1* (fig. 1(b)) and *QPC2* (fig. 1(c)), while for *QPC3*, in which the current flows perpendicular to the magnetic field, no spin-splitting is discernible up to 13 T (fig. 1(d)). Similar effects were observed on five other QPCs [15]. Note that *QPC2*, oriented parallel to the magnetic field, seems to have a larger splitting compared to *QPC1* which has a 45° angle with the field. Additionally, while the first subband of *QPC2* does not split, consistently with our data acquired on other QPCs oriented parallel to the in-plane field, it does split in *QPC1*.

Table 1 quantifies the splitting of the spin subbands displayed in fig. 1. The width of the lines is the main source of error. For the first subband in *QPC2* and the subbands of *QPC3* an upper bound for the splitting is indicated which is based on the width of these lines.

Calculation of the lever arms. The common approach to calculate the g-factor is based on the source-drain bias voltage corresponding to the 1D subband separation, divided by the magnetic field at which the spin-split subband crossings occur [7–10]. Due to the strong confinement in our QPCs, however, the subband splitting is a factor of 2–3 larger than the figures reported in the above-mentioned references and no crossing of spin-split levels happens up to a magnetic field of 13 T. Therefore, we use a different approach which requires an independent determination of gate lever arms from the finite-bias spectra, to transform the gate voltage axes in fig. 1 to an energy axis.

The finite-bias differential conductance ($\mathrm{d}I/\mathrm{d}V$) of *QPC1* is shown in fig. 2(a). Numbers in the figure indicate the differential conductance of different plateaus. A zero-bias anomaly (ZBA) is observed in this QPC as indicated by the black arrows. For the purpose of determining the lever arm, it is more convenient to follow the transconductance plot which is obtained from $\mathrm{d}I/\mathrm{d}V$ by a numerical derivative with respect to the gate voltage. The result is shown in fig. 2(b) for *QPC1* and in figs. 2(c), (d) for the other two QPCs. Bright areas in these plots represent the plateaus with differential conductances indicated in the figure in units of $2e^2/h$. The dark regions highlighted by dashed lines are transitions between the plateaus due to subbands entering or leaving the bias window. The white dashed lines mark the alignment of the subbands with the electrochemical potential of source and drain. The blue and green dashed lines show the evolution of the first subband with the applied bias which is anomalous (as if only one subband crosses the source while two subbands cross the drain) due to the presence of the 0.7 feature [16]. Therefore, we do not consider the first subband and the gray dashed line, which can be probably attributed to "0.7 Analogues" [17], in our analysis in this article.

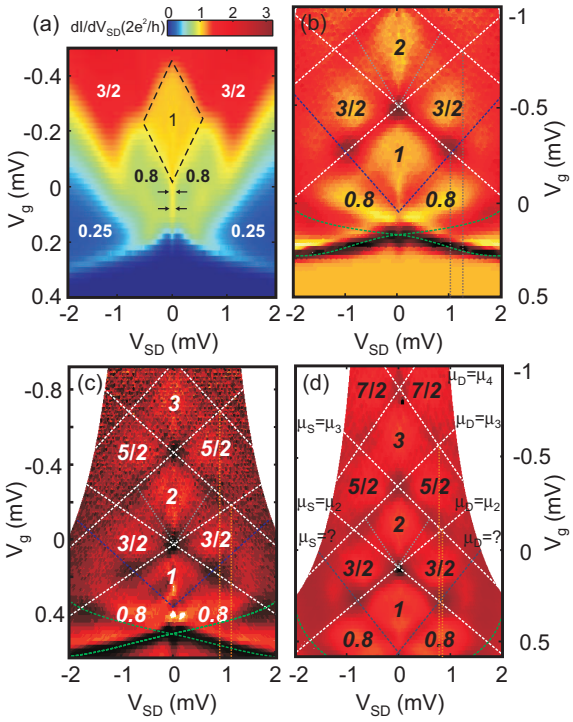

Fig. 2: (Color online) (a) Differential conductance of *QPC1* as a function of the gate voltage and the applied source-drain bias at $T = 100$ mK. A strong zero-bias peak is present as indicated by the arrows. (b)–(d): transconductance (numerical derivative of the differential conductance with respect to the gate voltage) in arbitrary units for *QPC1*, *QPC2* and *QPC3*, respectively. Bright areas are plateaus whose non-linear–conductance values are indicated in the figure in units of $2e^2/h$. Dashed lines mark the alignment of the subbands with the electrochemical potentials of the source and drain electrodes.

Vertical dashed lines in figs. 2(b)–(d) evaluate the bias at which the electrochemical potential of source and drain are aligned with two subsequent subbands and therefore give the subband splittings as eV. As a general trend, the subband splitting gets slightly smaller as the constriction

Table 2: The energy spacing between consecutive subbands $\Delta E_{n,n+1}$, evaluated from the position of the vertical dashed lines and the gate lever arm α_n on subband n. The lever arms are calculated from the slopes of the white dashed lines in fig. 2. The numbers in parentheses are the errors.

	QPC1	*QPC2*	*QPC3*
$\Delta E_{2,3}$ (meV)	1.32(±0.05)	1.14(±0.05)	0.89(±0.02)
$\Delta E_{3,4}$ (meV)		0.89(±0.05)	0.77(±0.03)
α_2 (meV/V)	2.6(±0.2)	2.6(±0.3)	2.5(±0.2)
α_3 (meV/V)	1.8(±0.1)	1.9(±0.2)	1.7(±0.1)
α_4 (meV/V)		1.7(±0.2)	1.4(±0.1)

opens up toward more negative gate voltages. This results also in a change in the slope of the white dashed lines as one moves toward more negative gate voltages. Table 2 summarizes the subband splittings and gate lever arms $\alpha_n = 0.5\mathrm{d}V_{SD}(n)/\mathrm{d}V_g(n)$ obtained from the slope of the white dashed lines for subband n averaged between the source and the drain lines.

In-plane anisotorpy of the Zeeman splitting. The above results can be combined to obtain the Zeeman spin-splitting energies per tesla, from which the g-factor can be calculated. According to eq. (1) we have

$$g_n^* = \frac{\alpha_n}{\mu_B}\frac{\mathrm{d}V_g(n)}{\mathrm{d}B}. \tag{2}$$

The g-factors are listed in table 3. Only the absolute values of the g-factors are stated here as their sign cannot be deduced from our experiment. The results obtained on two further samples *QPC4* and *QPC5*, measured with current aligned parallel to the magnetic field [16] are also included in this table.

While our measurements are in qualitative agreement with these results, a number of quantitative differences must be emphasized. We obtain 2–3 times larger values of the g-factor compared to those reported in [10]. As discussed in the next section this might be attributed to the strong confinement which results in subband splittings that are larger than those of quantum wires studied by Chen *et al.* [10]. This large subband spacing and the leakage-limited gate voltage range is the reason why only a few subbands are observed in our experiments. In contrast to those measured in *QPC2* and *QPC3* we obtain a non-zero Zeeman splitting for the first subband in *QPC1*, although a numerical value of the g-factor cannot be assigned to the first subband due to the ambiguity in extracting the lever arm.

Possible explanations. Within a theoretical framework, the anisotropy terms in the Hamiltonian for a 2DHG that would result in a linear-in-$B_\parallel$ spin-splitting at $\vec{k}_\parallel = 0$ are absent in (001)-oriented quantum wells. However, a substantial linear spin-splitting can be achieved due to the HH-LH mixing at $\vec{k}_\parallel = (k_x, k_y) \neq 0$ [3,10]. To linear oder

Table 3: g-factor of the 1D subbands. Data obtained on two further samples *QPC4* and *QPC5* with current directions oriented parallel to the magnetic field [15] are also included. The numbers in parentheses are the errors.

	QPC1 $B \angle 45° I$	*QPC2* $B \parallel I$	*QPC3* $B \perp I$	*QPC4* $B \parallel I$	*QPC5* $B \parallel I$
g_2	0.55(±0.05)	0.75(±0.1)	<0.05	0.45(±0.1)	0.6(±0.1)
g_3		0.8(±0.1)	<0.05	0.65(±0.1)	0.4(±0.05)
g_4			<0.05	0.95(±0.1)	

in $B_\parallel$ the Hamiltonian for a 2DHG is [3]

$$\begin{aligned}\mathcal{H}^{HH}_{[001]} &= z_{51}\mu_B\left(B_x k_x^2\sigma_x - B_y k_y^2\sigma_y\right)\\ &+ z_{52}\mu_B\left(B_x k_y^2\sigma_x - B_y k_x^2\sigma_y\right)\\ &+ z_{53}\mu_B\left\{k_x, k_y\right\}\left(B_y\sigma_x - B_x\sigma_y\right) + \mathcal{O}(B_\parallel^3),\end{aligned} \tag{3}$$

where $\hbar\vec{k} = -i\hbar\vec{\nabla}$ is the momentum operator and the z parameters are constants given by

$$\begin{aligned} z_{51} &= -1.5\kappa\gamma_2\mathcal{Z}_1 + 6\gamma_3^2\mathcal{Z}_2,\\ z_{52} &= +1.5\kappa\gamma_2\mathcal{Z}_1 - 6\gamma_3\gamma_2\mathcal{Z}_2,\\ z_{53} &= +3.0\kappa\gamma_3\mathcal{Z}_1 - 6\gamma_3(\gamma_2+\gamma_3)\mathcal{Z}_2.\end{aligned}$$

γ_1, γ_2 and γ_3 are Luttinger parameteres [3] which are equal to 6.85, 2.10 and 2.90 in GaAs, respectively. $\kappa = 1.2$ is the bulk valence band g-factor. Parameters $\mathcal{Z}_1$ and $\mathcal{Z}_2$ quantify the bulk and QW confinement contributions to the HH-LH mixing and depend on the actual form of the confinement potential of the 2DHG (see the appendix).

In 1D systems the transverse quantization of the wave vectors amplifies one of the k_x or k_y on the expense of the other and thus boosts up the corresponding terms in the above Hamiltonian. For a current flowing in the x-direction (100) with $\psi \propto \phi_n(y)e^{ik_x x}$, an order of magnitude estimate of the transverse wave vector k_y can be calculated from the zero-field subband energies while $k_x \approx 0$ at the onset of the opening of a subband as seen in the linear-conductance measurements. With this substitution only the terms $\langle k_y^2\rangle\left(-z_{51}B_x\sigma_x + z_{52}B_y\sigma_y\right)$ contribute to the spin-splitting. The g-factor proportionality to the cumulative subband spacing through $\langle k_y^2\rangle$ explains why the values of the g-factors mostly increase for higher subbands and why our g-factors are higher than those obtained on quantum wires with a weaker confinement [10]. Note that for a wide QPC, $\langle k_y^2\rangle \to k_F^2 \propto n_s$ and the g-factors saturate at a value proportional to the density.

The origin of the confinement anisotropy is, however, more subtle and cannot be directly obtained from the above quasi-1D considerations [10]. In order to demonstrate this, we rotate 45° to the x' and y' axes along the [110] and [1$\bar{1}$0] directions and obtain

$$g^*_{B\parallel I} = 3\gamma_3\left\langle k_{y'}^2\right\rangle\left|\kappa\mathcal{Z}_1 - 4\gamma_3\mathcal{Z}_2\right|, \tag{4}$$

$$g^*_{B\perp I} = 3\gamma_3\left\langle k_{y'}^2\right\rangle\left|\kappa\mathcal{Z}_1 - 4\gamma_2\mathcal{Z}_2\right| \tag{5}$$

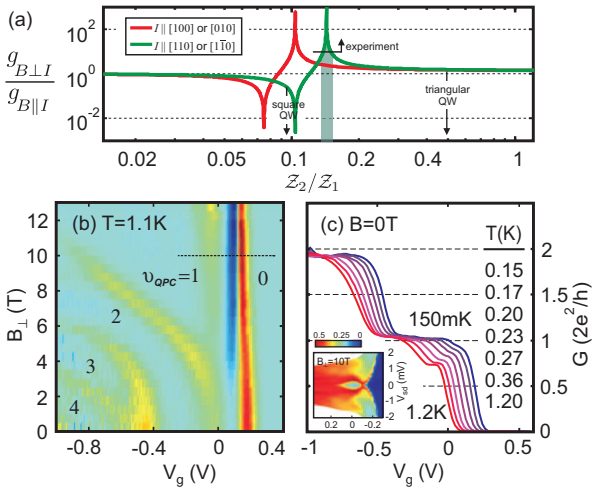

Fig. 3: (Color online) (a) The ratio of g-factors for in-plane fields along and perpendicular to the QPC axis as a function of $\mathcal{Z}_2/\mathcal{Z}_1$ for two different directions of the current with respect to the crystallographic axes. Our measurements suggest $\mathcal{Z}_2/\mathcal{Z}_1 \approx 0.15$ which is different from the corresponding values of square and triangular QWs. (b) Transconductance (numerical derivative with respect to the gate voltage) of *QPC1* with arbitrary unit as a function of gate voltage and magnetic field perpendicular to the plane measured at $T = 1.1\,\mathrm{K}$. Light-blue areas are plateaus whose filling factors are indicated in the figure. Red and yellow lines are transitions between these plateaus as the subbands pass the Fermi energy. (c) Temperature dependence of the linear conductance for *QPC1* confirming the presence of the 0.7 feature in this QPC. The inset shows the differential conductance along the black dashed line in (b) at $B_\perp = 10$ T, showing a Coulomb blockade-like diamond of suppressed conductance.

for the absolute values of the g-factors, independently of the two crystallographic directions [110] and [1$\bar{1}$0]. The ratio of these two g-factors depends only on $\mathcal{Z}_2/\mathcal{Z}_1$ and is plotted in fig. 3(a) for two different current directions with respect to the crystallographic directions. In the context of the above quasi-1D theory, our experimental observation of $g^*_{B\parallel I} \gg g^*_{B\perp I}$ requires a value of $\mathcal{Z}_2/\mathcal{Z}_1 \approx 0.15$. We have calculated this parameter for both square and triangular QW confinements and indicated the values in the figure (see the appendix). While the predictions of the quasi-1D theory with a triangular QW (in contrast to a square QW and as anticipated by [11]) gives the correct trend ($g^*_{B\parallel I} > g^*_{B\perp I}$), it does not explain the large ratio that is obtained by the measurements. However, the contrast between square and triangular QWs points to the sensitivity of the results on the shape of the hole wave functions. A precise determination of $\mathcal{Z}_2/\mathcal{Z}_1$ requires a more detailed self-consistent calculation which is beyond the scope of the present work. Nevertheless, an experimental test of the quasi-1D theory would be to repeat the experiment in QPCs with a current oriented along the [100] and [010] directions. The quasi-1D theory predicts a much smaller g-factor anisotropy in that case, as can be seen from the comparison of the red and green curves in fig. 3(a) at the experimentally concluded value of $\mathcal{Z}_2/\mathcal{Z}_1 \approx 0.15$.

Out-of-plane magnetic field. Similar experiments can be performed to observe the Zeeman splitting in a magnetic field perpendicular to the plane of the 2DHG. Figure 3(b) shows the transconductance of *QPC1* measured in this particular field direction. A $B_\perp$-dependent series resistance is subtracted from the raw data to account for orbital effects in the leads [18]. The filling factors on different plateaus are indicated in the figure. In addition to the Zeeman spin-splitting of the subbands, an orbital shift due to the formation of magnetoelectric subbands [19] is present in these data. Therefore, to determine the g-factor, one has to consider the low magnetic field regime in which the cyclotron energy is much smaller than the subband splitting. Moreover, the classical cyclotron radius in our system is 100 nm/tesla, implying that the wave functions are strongly influenced by the magnetic field already at a few tesla and the zero-field lever arms extracted from fig. 2(b) are no longer valid. Nevertheless, reading the spin-splitting of $\mathrm{d}V_g(2)/\mathrm{d}B \approx 0.11$ of the second subband (the first subband is anomalous because of the presence of the 0.7 anomaly) from the low-field ($B_\perp < 2T$) part of fig. 3(b) and using the zero-field lever arm of $\alpha_2 \approx 2.6$ as listed in table 2 give a perpendicular g-factor of $g_\perp \approx 5$. The same number has been recently obtained by a different group [20]. For comparison the theoretical perpendicular g-factor of holes in 2D is $g^{HH}_\perp = 6\kappa \approx 7.2$ [3] which is closer to our result than the previously reported $g_\perp \sim 2$ values measured by optical techniques [21,22].

0.7 anomaly. Finally we shortly discuss here the 0.7 anomaly which is omnipresent in the p-type GaAs QPCs studied here [18]. As was shown before, *QPC1* exhibits a strong ZBA in the differential conductance (fig. 2(a)). Moreover, in fig. 3(b) the spin-split branches of the first subband remain gapped in the limit of zero magnetic field at the elevated temperature of 1.1 K, which is a signature of the 0.7 anomaly. The evolution of this gap to a blue stripe (negative transconductance) at finite fields ($B_\perp > 4$ T) points to a peaked (non-monotonous) linear conductance, as was first shown in [18], and was interpreted as the signature of a quasi-bound state forming in the QPC. The temperature dependence of the linear conductance in *QPC1* presented in fig. 3(c) confirms the presence of a clear 0.7 anomaly [17]. The inset shows the finite-bias differential conductance along the dashed line in fig. 3(b), testifying that the conductance peak is accompanied by a diamond-like region of suppressed conductance reminiscent of a Coulomb diamond in quantum dots [18].

Conclusion. – We have studied the in-plane and out-of-plane anisotropy of the Zeeman spin-splitting in hole QPCs. It is shown that the g-factor is zero if the in-plane magnetic field is applied perpendicular to the current direction. The results presented here are in qualitative agreement with the work presented in refs. [7,9,10]. The g-factor values are, however, higher than those reported

in previous works. The role of the confinement in the enhancement of the g-factor was discussed and it was shown that although arguments based on the 2D theory [3] can qualitatively explain the observed features, a quantitative understanding is still missing. The signatures of the 0.7 anomaly in the data have been discussed and the out-of-plane g-factor was estimated, providing values which are closer to theory than those reported earlier.

* * *

We thank the Swiss National Science Foundation for financial support. MC is a grantee of the János Bolyai Research Scholarship of the HAS and acknowledges financial support of the European Union 7th Framework Programme (Grant No. 293797). DR and ADW acknowledge support from DFG SPP1285 and BMBF QuaHL-Rep 01BQ1035.

Appendix

In this appendix we calculate the HH-LH mixing parameters $\mathcal{Z}_1$ and $\mathcal{Z}_2$ for quantum wells with deep square and triangular potentials (particle in a box). These parameters are given by the perturbation theory [3]

$$\mathcal{Z}_1 = \frac{i\hbar^2}{m_0}\frac{\langle h_1|\,[k_z,z]\,|l_1\rangle\,\langle l_1|h_1\rangle + \langle h_1|l_1\rangle\,\langle l_1|\,[k_z,z]\,|h_1\rangle}{E_1^h - E_1^l},$$
$$\mathcal{Z}_2 = \frac{i\hbar^2}{m_0}\sum_n \frac{\langle h_1|\,k_z\,|l_n\rangle\,\langle l_n|\,z\,|h_1\rangle - \langle h_1|\,z\,|l_n\rangle\,\langle l_n|\,k_z\,|h_1\rangle}{E_1^h - E_n^l}.$$

In case of a square potential well with a width w we obtain

$$\mathcal{Z}_1 = \frac{w^2}{\pi^2\gamma_2}, \qquad \mathcal{Z}_2 = \frac{512w^2}{27\pi^4(3\gamma_1+10\gamma_2)}$$

to the leading order, which agree with [3] and give $\mathcal{Z}_2/\mathcal{Z}_1 = 0.097$ independently of the QW width w. To see the sensitivity of this result to the exact form of the wave function, we calculate the $\mathcal{Z}_2/\mathcal{Z}_1$ for an infinite triangular QW. The eigen energies and wave functions are

$$E_n = -\frac{\hbar^2\alpha^2}{2m_0}\eta a_n, \qquad \varphi_n(z) \propto Ai\left(\eta^{-1}\alpha z + a_n\right),$$

where $a_n = -\left[3\pi/2(n-1/4)\right]^{2/3}$ are the zeros of the Airy function and $\eta^3 = m_0/m^*$. The parameter $\alpha = \sqrt[3]{2m_0e^2n_s/2\epsilon\hbar^2}$ contains all the density dependence of the wave function and can be taken out of the matrix elements by a change of the variable $y = \alpha z$. Substitution of these eigen functions and energies into the above formula, thus results in integrals that can be computed numerically. Although the HH-LH mixing parameters $\mathcal{Z}_1$ and $\mathcal{Z}_2$ depend on the density through $\mathcal{Z} \propto \alpha^{-2} \propto n_s^{-2/3}$, their ratio $\mathcal{Z}_2/\mathcal{Z}_1 \approx 0.5$ is density independent.

REFERENCES

[1] Ashcroft N. W. and Mermin N. D., *Solid State Physics* (Brooks Cole) 1976.
[2] Madelung O., *Semiconductors - Basic Data* (Springer) 1996.
[3] Winkler R., *Spin-orbit Coupling Effects in Two Dimensional Electron and Hole Systems* (Springer) 2003. See `http://www.niu.edu/rwinkler/research/stmp.pdf` for a list of corrections.
[4] Winkler R., Culcer D., Papadakis S. J., Habib B. and Shayegan M., *Semicond. Sci. Technol.*, **23** (2008) 114017.
[5] Habib B., Shayegan M. and R. Winkler, *Semicond. Sci. Technol.*, **24** (2009) 064002.
[6] Winkler R., Papadakis S. J., De Poortere E. P. and Shayegan M., *Phys. Rev. Lett.*, **85** (2000) 4574.
[7] Danneau R., Klochan O., Clarke W. R., Ho L. H., Micolich A. P., Simmons M. Y., Hamilton A. R., Pepper M., Ritchie D. A. and Zülicke U., *Phys. Rev. Lett.*, **97** (2006) 026403.
[8] Koduvayur S. P., Rokhinson L. P., Tsui D. C., Pfeiffer L. N. and West K. W., *Phys. Rev. Lett.*, **100** (2008) 126401.
[9] Klochan O., Micolich A. P., Ho L. H., Hamilton A. R., Muraki K. and Hirayama Y., *New J. Phys.*, **11** (2009) 043018.
[10] Chen J. C. H., Klochan O., Micolich A. P., Hamilton A. R., Martin T. P., Ho L. H., Zülicke U., Reuter D. and Wieck A. D., *New J. Phys.*, **12** (2010) 033043.
[11] Held R., Vancura T., Heinzel T., Ensslin K., Holland M. and Wegscheider W., *Appl. Phys. Lett.*, **73** (1998) 262.
[12] Hirayama Y., Wieck A. D. and Ploog K., *J. Appl. Phys.*, **72** (1992) 3022.
[13] Wieck A. D. and Reuter D., *Inst. Phys. Conf. Ser.*, **166** (2000) 51.
[14] Csontos M., Komijani Y., Shorubalko I., Ensslin K., Reuter D. and Wieck A. D., *Appl. Phys. Lett.*, **97** (2010) 022110.
[15] Komijani Y., PhD Thesis (ETH Zürich) 2012.
[16] Micolich A. P., *J. Phys.: Condens. Matter*, **23** (2011) 443201.
[17] Graham A. C., Thomas K. J., Pepper M., Simmons M. Y., Ritchie D. A., Berggren K.-F., Jaksch P., Debnarova A. and Yakimenko I. I., *Solid State Commun.*, **131** (2004) 591.
[18] Komijani Y., Csontos M., Shorubalko I., Ihn T., Ensslin K., Meir Y., Reuter D. and Wieck A. D., *EPL*, **91** (2010) 67010.
[19] Beenakker C. W. J. and van Houten H., *Solid State Phys.*, **44** (1991) 1.
[20] Srinivasan A., Yeoh L. A., Klochan O., Martin T. P., Chen J. C. H., Micolich A. P., Hamilton A. R., Reuter D. and Wieck A. D., *Nano Lett.*, **13** (2013) 148.
[21] Sapega V. F., Cardona M., Ploog K., Ivchenko E. L. and Mirlin D. N., *Phys. Rev. B*, **45** (1992) 4320.
[22] van Kesteren H. W., Cosman E. C., van der Poel W. A. J. A. and Foxon C. T., *Phys. Rev. B*, **41** (1990) 5283.